Bulletin of the JSME Vol.17, No.1, 2023
Journal of Advanced Mechanical Design, Systems, and Manufacturing

Optimization of fast tool servo diamond turning for enhancing geometrical accuracy and surface quality of freeform optics

Lin ZHANG*, Yusuke SATO* and Jiwang YAN*
* Department of Mechanical Engineering, Faculty of Science and Technology, Keio University
3-14-1, Hiyoshi, Kohoku-ku, Yokohama, 223-8522, Japan
E-mail: yan@mech.keio.ac.jp

Received: 30 May 2022; Revised: 8 August 2022; Accepted: 5 October 2022

Abstract
Fast tool servo (FTS) in ultra-precision diamond turning is an efficient technique for high-precision fabrication of freeform optics. However, the currently adopted constant scheme for control point sampling takes no account of the shape variation of the desired surface, which might lose some micro features and result in low form accuracy and non-uniform surface quality. Facing this issue, this manuscript proposes a novel adaptive control points sampling strategy, which improves the form accuracy and keeps as many as the micro surface features. In the optimization method, the sampling stepovers between two adjacent control points are actively adjusted to adapt to the surface profile variation. By adopting this method, the control point sampling induced interpolation error is constrained within the desired tolerance and eliminates the lack/over-definition of control points in the machining area. The feasibility of the proposed optimization method is demonstrated by both theoretical simulations and fabrication experiments of sinusoid freeform surfaces. Compared with the constant sampling method, both the theoretical predicted and experimental measured form error of the proposed method is remarkably reduced by about 35 % with the same amount of control points. This technique provides a new route to allocating control points in FTS diamond turning to achieve high form accuracy and machining efficiency in the fabrication of freeform optics.

Keywords: Fast tool servo, Diamond turning, Adaptive control point, Freeform surface, Form accuracy

1. Introduction

A freeform optical surface, designed with little to no symmetry, is generally regarded as a disruptive evolution of the optical system, since it constitutes a powerful tool offering the possibility to enhance the optical performance or compact the volume of optical systems compared with conventional designs, or a combination of these two attractive features (Jiang et al., 2007; Kim et al., 2021; Roland et al., 2019). Recently, the increasing applications of freeform optics in imaging and non-imaging optical instruments stimulated a great demand for the fabrication of intricate freeform optics with high form accuracy, surface quality and machining efficiency (Fang et al., 2013; Bauer and Rolland, 2014). Fast tool servo (FTS) diamond turning is regarded as one of the most promising techniques due to its superior capability on sub-micro form accuracy, nanoscale surface roughness and high machining efficiency (Kim et al., 2009; Zhang et al., 2013; Tanikawa and Yan, 2022). Recently, considerable effort has been made to optimize the processing conditions, improve the form accuracy and enhance the machining efficiency, including the machining parameter optimization (cutting speed, feed rate and depth of cut) (Yu et al., 2011; Scheiding et al., 2011), optimal toolpath determination (Zhu and To, 2015; Sato and Yan, 2022), and static and dynamic motion-induced error compensation (Lu and Trumper, 2007; Yu et al., 2012). With the aid of these techniques, the form accuracy and surface roughness in FTS diamond turning has been significantly improved on many engineering materials (Zhang et al., 2021; Zhu et al., 2015).

For mechanical machining, the relative motion between the tool and the workpiece is utilized to carve out the contour of the desired surface. Different from the slow tool servo (STS) diamond turning, in which the servo motions of the three axes (x-, z- and c-axis) are synchronously controlled by the machine tool and the tool position is determined by linear interpolation based on the successive control points on a spiral toolpath, the independent FTS unit possesses a separate

Paper No.22-00227
[DOI: 10.1299/jamdsm.2023jamdsm0012]

controller with a novel strategy to drive the diamond tool for high flexibility and rapid response, as shown in Fig. 1(a). To distinguish the *z*-axis motion of the machine tool from the FTS unit, the *z*-axis motion of the FTS unit is generally called the *w*-axis. As an independent unit, the FTS controller consists of a signal amplifier and a succession of driven units, which are employed to collect the notification and feedback, adjust the signal in real-time and enable the diamond tool with a nanometric step revolution. Besides, the unidirectional communication between the machine tool and the FTS controller further sets a higher request for processing capacity and rapid response, since the FTS unit has to follow up the motion of the machine tool closely. After the data has been collected by the FTS controller, it is consolidated, organized and processed into easy-to-read summary commands to drive the diamond tool. Since the *z*-axis motion of the machine tool is completely replaced with the *w*-axis motion of the FTS unit, the *z*-axis slide remains in a constant position in the FTS diamond turning operation, and the spatial control point cloud of the desired surface is preserved in the FTS controller, which is further used for tool positioning, as shown in Fig. 1(b). To improve the responding ability and speed, the speed of data processing is increased and available for subsequent processing and handling on account of the optimizing data structure of the control point cloud. Deriving from this, the structure of the control point cloud in the FTS controller has to be satisfied with at least two essential requirements: (a) the volume of the control point cloud should be fit for the storage space and easily managed by the FTS controller, since too many control points will remarkably slow down the system response and reduce the control accuracy (Gao et al., 2003); and (b) the control points should be well-organized for fast positioning and easy search.

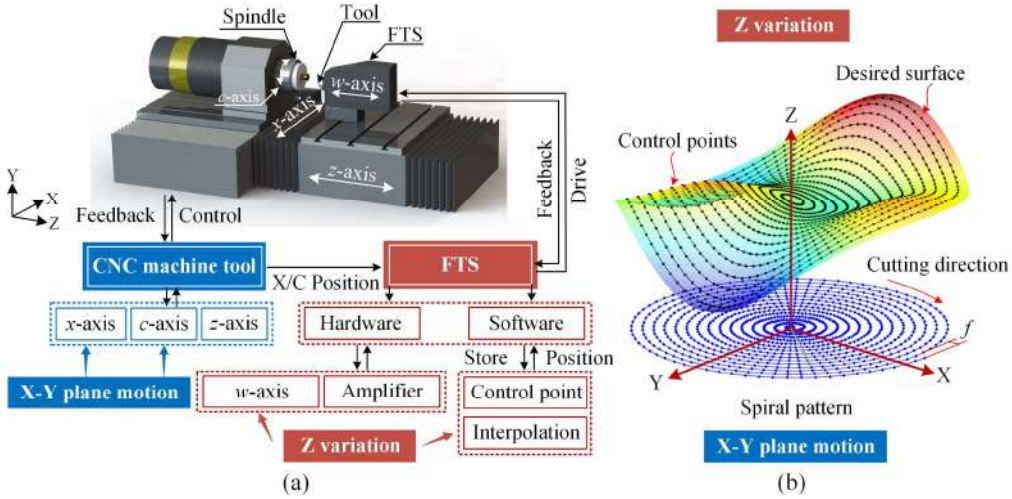

Fig. 1 (a) The hardware configuration and control flow between the machine tool and the FTS unit, and (b) different control point patterns stored in the machine tool and the FTS unit.

Generally, two kinds of control point sampling strategies are mainly adopted in STS diamond turning, including the constant-angle sampling strategy (CASS) and the constant-arc-length sampling strategy (CALS). Since the CASS allocates the same amount of control points per revolution from the center to the edge, it has become a more commonly used sampling method in diamond turning. Although it is sufficient for small radii, the low angular coordinate density for large radii can not fully meet the requirement of form accuracy. Because the interpolation error is highly dependent on the arc length between the control points, it can hardly be suppressed within the desired tolerance with increasing radius. To guarantee sufficient control points at large radii, angular subdivision should be performed, which, in turn, results in over-defined control points concentrated around the center point, significantly increasing the machining time and the volume of the program (Yu et al., 2011). In addition, it will significantly slow down the response of the control system due to the intricate interpolation and servo time of the physical system, which easily leads to the asynchronization of the physical motions of the slides (Neo et al., 2014). The CASS, while simple and convenient to compute, does not provide enough flexibility and applicability for the machining areas of various radii. To overcome the difficulties and achieve uniform sampling, in STS diamond turning, a hybrid sampling strategy that combines the CASS and CALS was proposed (Neo et al., 2014; Zhou et al., 2010), which utilizes an equal angle spiral for small radii and an equal arc length spiral for large radii. However, this strategy is no longer suitable for the independent FTS unit.

Another critical factor in the form error is the surface shape variation. For the freeform surface, the surface shape variation will lead to remarkable interpolation errors at different cutting points. Thus, the CASS or CALS, regardless of

[DOI: 10.1299/jamdsm.2023jamdsm0012]

surface shape variation, inevitably results in a heterogeneous distribution of interpolation error on the finished surface. To enhance the freeform surface accuracy, an adaptive diamond turning method, fully considering the cutting-forward and side-feeding motion induced the form error with various surface shape variations, was proposed and demonstrated in STS diamond turning (Zhu and To, 2015). Although the adaptive diamond turning method has superiority in generating high-precision freeform surface, the computation load is significantly increased, compared with the commonly used CASS and CALS. In addition, this method, re-locating the control points from the spiral toolpath, induces high-frequency vibration into the x-axis, which loses flexibility and suitability for most commercial one-dimensional (1D) FTS units.

Facing this issue, a novel control point sampling strategy should be introduced to satisfy the requirements of the independent FTS units. In this research, variable stepovers between the successive control points are introduced to improve the form accuracy and surface quality while maintaining a well-organized data structure of the control point cloud. Thereby, the adaptive control point sampling (ACPS) strategy is proposed with full consideration of the interpolation error due to the surface shape variation in FTS diamond turning. Initially, the optimization principle and strategy of the ACPS method are presented in detail. Then, both numerical simulations and diamond turning experiments are conducted to evaluate the effectiveness of the ACPS method. Finally, by comparing the form accuracy and surface quality of the machined surfaces, the ACPS method demonstrates its superiority beyond the constant sampling method. The present study provides a new way to improve surface form accuracy and machining efficiency simultaneously in freeform surface fabrication.

2. Methodology

2.1 FTS control system and strategy

In FTS diamond turning, the process is generally performed in a cylindrical coordinate system (ρ, θ, z), in which the diamond tool follows a spiral motion. The motion component along the tangent line is regarded as the cutting-forward direction, while the polar axis direction is viewed as the side-feeding direction (Nagayama and Yan, 2021). The z-axis servo motion is utilized to carve out the contour of the desired surface. For the STS diamond turning, the three spatial coordinates, including ρ, θ and z, are determined in toolpath generation and kept in the machine tool. The physical motions of x-, c- and z-slides follow each positioning command to complete the machining process. In FTS diamond turning, the control strategy is completely different from that in STS diamond turning. The motions of the x-, c- and z-axis are separated into two parts. The spiral motion in the x-y plane is completed by the physical motions of the x- and c-slide of the machine tool, while the FTS unit is only responsible for the motion of the w-axis. Therefore, the control point cloud in the machine tool is a two-dimensional (2D) spiral pattern, similar to the toolpath in STS diamond turning except for the motion of the z-axis, whereas the control point cloud in the FTS unit is utilized to describe the three-dimensional (3D) contour of the desired surface, regardless of the physical motion of the diamond tool in the x-y plane. In general, there are mainly two kinds of geometrical patterns for FTS units on control point sampling, which take both accuracy and availability into consideration, namely ring pattern and mesh pattern, as shown in Fig. 2.

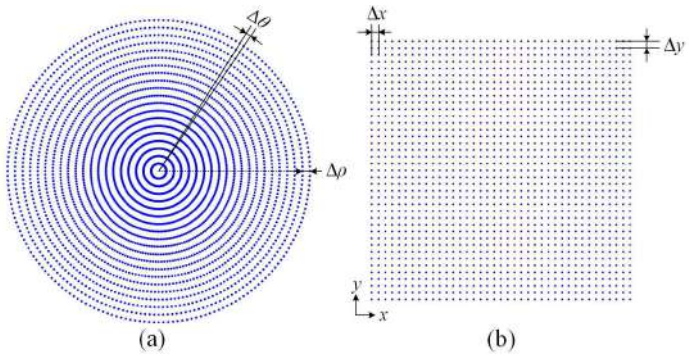

Fig. 2 Schematic diagrams of control point sampling patterns, including the (a) ring pattern and (b) mesh pattern.

For the ring pattern, the control points are uniformly allocated on a series of concentric circles with a constant pitch $\Delta\rho$ and angular stepover $\Delta\theta$, as illustrated in Fig. 2(a), which are regarded as crucial geometrical parameters for control point sampling. Similarly, the control points allocated in the mesh pattern form a rectangular design, and the Δx and Δy are the stepovers along the x- and y-axis, respectively. In FTS diamond turning, the real-time x- and c-axis positions are

[DOI: 10.1299/jamdsm.2023jamdsm0012]

gathered by the grating encoders of the machine tool, which are sent to the FTS controller within several microseconds and employed as input for the FTS command generator. After a series of data processing, a group of control points, which are close to the cutting position, is extracted from the control point cloud preserved in the FTS unit. Then, the *w*-axis position of the diamond tool is determined by the bilinear-interpolation method, and the corresponding command is further adjusted by the PID controller and amplifier to drive the diamond tool.

2.2. Interpolation method and form error

For the desired freeform surface with determined diamond tool geometry, the primary controllable factors that determine the machined form accuracy and surface quality are the interpolation method, sampling density and the side-feeding induced residual tool marks, as illustrated in Fig. 3. As an essential factor in machined surface accuracy, the interpolation method does not exert the same effect as other factors, which commonly influences the form accuracy with surface shape variation and control point density. In FTS diamond turning, the *w*-axis position of the diamond tool is obtained based on the bilinear-interpolation method using the nearby control points due to its simple computation and fast response, as shown in Fig. 3(a). The *w*-axis position of the diamond tool can be described as follows,

$$w = (1-t)(1-u)w_{i.j} + t(1-u)w_{i+1,j} + tuw_{i+1,j+1} + (1-t)uw_{i,j+1} \tag{1}$$

where t and u between 0 to 1 are given as,

$$t = \frac{(x - x_i)}{(x_{i+1} - x_{i-1})} \tag{2}$$

$$u = \frac{(y - y_i)}{(y_{i+1} - y_{i-1})} \tag{3}$$

Along the cutting-forward direction, as shown in Fig. 3(b) and 3(c), the interpolation error is due to the gap between the desired surface and the interpolation surface, which can be classified into two kinds of form errors in terms of the positive/negative of the deviations: (a) the convexity induced over-cutting effect (negative), and (b) the concavity induced less-cutting effect (positive). Although some improved interpolation methods could effectively minimize the form error, the computation load is increased by several orders than the most commonly used linear methods (Dick et al., 2012; Scheiding et al., 2011). However, since the interpolation computation is a real-time operation, the complicated calculation procedures will lead to an extra burden on the controller that most of the FTS units could not afford. On the other hand, along the side-feeding direction, the tool motion will consistently achieve positive tool residual tool marks, as shown in Fig. 3(d). This form deviation is highly dependent on the feed rate and the radius of the diamond tool.

In FTS diamond turning, the side-feeding motion induced form error can be largely reduced by reducing the side-feeding rate f in the x-axis, which is thought to be unacceptable in the STS diamond turning due to the low machining efficiency. However, since the spindle speed in FTS diamond turning (100~600 rpm) is usually tens or hundreds of times higher than that used in STS diamond turning (5~30 rpm), the reduction in the side-feeding rate in the x-axis does not lead to a significant decline on machining efficiency. Based on the analysis above, the form accuracy and surface integrity are mainly affected by the sampling density and surface shape variation. Thus, the constant stepover without consideration of surface shape variation may not be suitable for intricated freeform surfaces, especially for some characters with high-frequency micro features. For the ACPS method, the sampling stepovers, regardless of the ring and mesh pattern, are deliberately determined to adapt to the surface shape variation. As shown in Fig. 4, in the constant control point sampling method, the machining area is divided into many sectors with constant angle θ_1 and the corresponding control points at different radii are marked with dark points. In the optimization, for instance, in Fig. 4(a), the machining error at the radius of r_1 is less than the tolerance, while the error at the radius of r_2 is larger than the desired tolerance. In order to keep the control points with the same angle stepover, the original control points at the radius of r_1 and r_2 should be moved close to the adjacent control points to reduce the machining error until within the tolerance. Thus, the angle stepover at this angle becomes smaller. Such situations also occur when the machining error is larger than the tolerance, as shown in Fig. 4(b) and 4(c). On the other hand, when the machining error is less than the tolerance, the control points can be moved further from each other, as shown in Fig. 4(d). By carefully allocating the control points, the

[DOI: 10.1299/jamdsm.2023jamdsm0012]

interpolation error can be constrained within the desired tolerance on the whole machining area. In this way, a much larger sampling stepover can be adopted with slight curvature variation and vice versa. Therefore, the required volume of control point for FTS diamond turning would be much smaller than that for the constant sampling method to achieve comparable machining accuracy and surface quality.

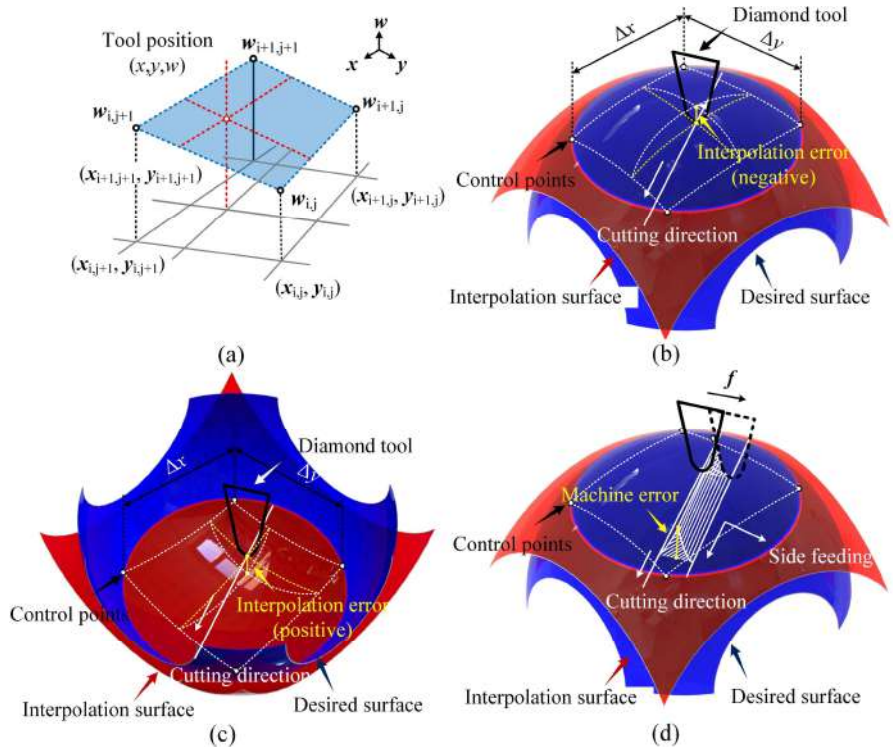

Fig. 3 Schematic diagrams of (a) the bilinear-interpolation method in tool position determination, the form error generation due to (b) convex surface variation, (b) concave surface variation, and (b) the side-feeding direction.

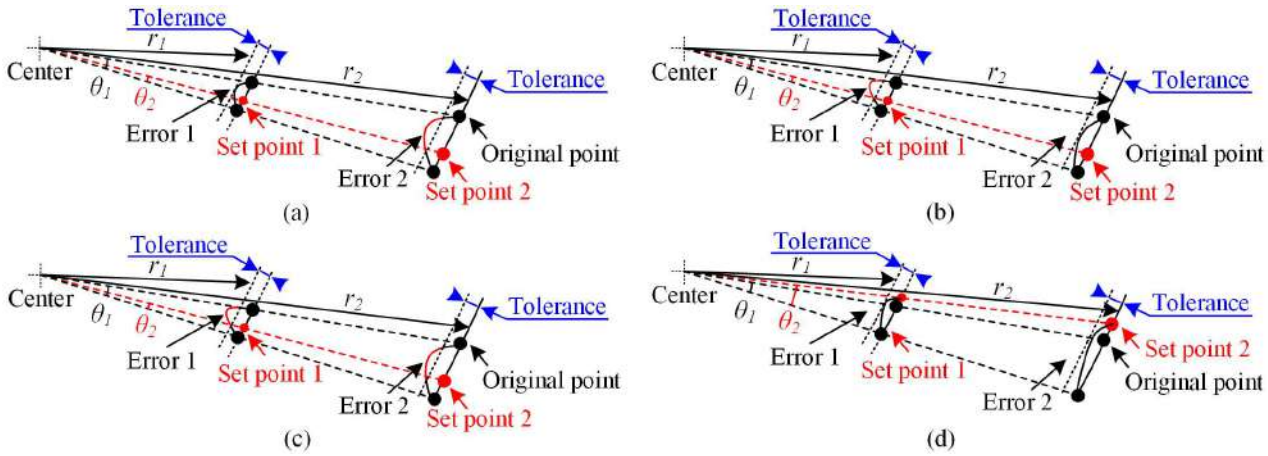

Fig. 4 Schematic diagrams of the optimization process with different situations, (a)-(c) machining error larger than the tolerance at r_1 or/and r_2, and (d) machining error less than the tolerance at r_1 and r_2.

2.3 Control point determination

As mentioned above, in both ring and mesh patterns, two crucial geometrical parameters must be optimized to satisfy the desired tolerance in two directions. Since the ACPS method does not disturb the original data structure of the control point cloud, *i.e.*, equivalent control points per revolution, the FTS unit will keep the same or even better processing speed and position accuracy. In order to enhance the calculation robustness, the optimization process for each parameter is completed in two uncoupled processes. In the following paragraph, the mesh pattern is demonstrated in the optimization

[DOI: 10.1299/jamdsm.2023jamdsm0012]

process as an example. Since the geometrical parameters (Δx and Δy) have the equivalence property, the order of optimization does not matter. Thus, the optimization is conducted with Δx and Δy consecutively.

At the initial stage, the machining area is homogeneously divided into small squares with Δx_{min} and Δy_{min} along x- and y-axes, which are treated as the smallest unit for Δx and Δy, as shown in Fig. 5(a). The stepovers between these candidate control points are much smaller than those in the constant sampling method (Δx_{nom}, Δy_{nom}). The initial sampling control points $p_{n,m}$ are marked with the row and column number, and the corresponding value on the desired surface can be expressed as $z_{n,m} = f(x_{n,m}, y_{n,m})$. Then, the optimization for Δx is initialized from $p_{1,1}$ to $p_{1,m}$ as shown in Fig. 5(b). For instance, the control points $p_{1,n}$ and $p_{1,n+2}$ ($1<n<m-2$) are selected from the sequence. Based on the linear interpolation along the y-axis, the predicted value $z'_{1,n+1}$ at the control point of $p_{1,n+1}$ can be determined and the deviation between the actual value $z_{1,n+1}$ and predicted value $z'_{1,n+1}$ can be calculated as $\varepsilon_{1,n+1} = | z_{1,n+1} - z'_{1,n+1} |$. If the obtained deviation $\varepsilon_{1,n+1}$ is larger than the desired tolerance ε_x, the point $p_{1,n+1}$ is chosen as the control point, which is further utilized as the initial point to determine the next control point. In the other case, when the obtained deviation $\varepsilon_{1,n+1}$ is less than the desired tolerance ε_x, the next point $p_{1,n+3}$ is selected and the deviations at the points of $p_{1,n+1}$ and $p_{1,n+2}$ are obtained. If either of the calculated deviations ($\varepsilon_{1,n+1}$, $\varepsilon_{1,n+2}$) does not satisfy the requirement on tolerance, the point $p_{1,n+2}$ is set as the control point. The control point is moved forward until the interpolation error between the initial point and the current point does not satisfy the requirement of the tolerance. The optimization flow of the control points is shown in Fig. 5(c). By iterating the process for all the candidate control points, the appropriate sampling stepovers Δx and Δy are determined based on the surface shape variation along the x- and y-axis. Considering the equivalent control points along each row and column, the minimum Δx and Δy should be selected from the columns and rows.

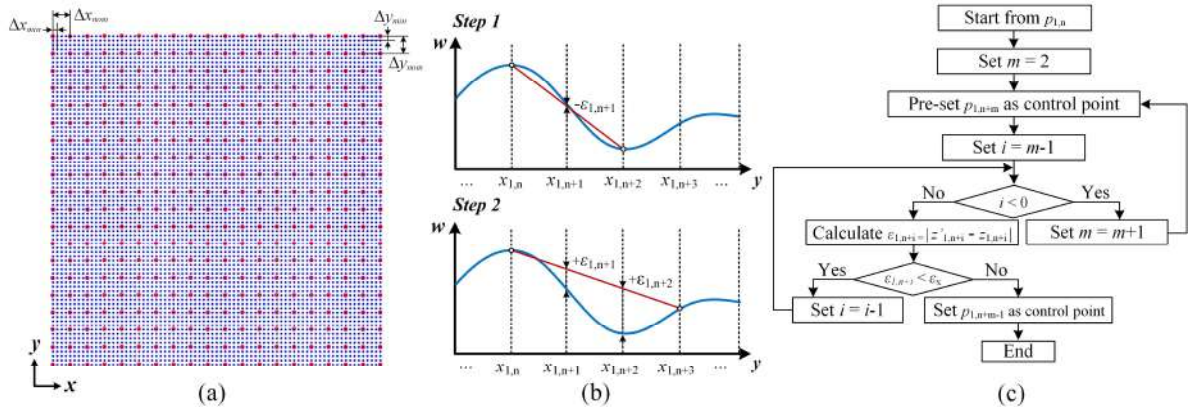

Fig. 5 Schematic diagrams of optimization process (a) initialization of candidate control point cloud, (b) determination principle, and (c) optimization flow for each candidate control point.

Instead of being constant, variable pitches $\Delta\rho$ and angular stepovers $\Delta\theta$ for the ring pattern can be obtained based on the desired surface. This allows the concentric circles with varying radii and arc length to be generated, which largely extends the capability of the control point cloud to precisely describe the contour of the freeform surface with the same or even less volume. The machining error can be effectively limited by non-uniformly distributed control points based on the desired surface profiles with high flexibility and excellent compatibility. Examples of ring patterns with various radial pitches and angular stepovers are shown in Fig. 6(a). For instance, in Fig. 6(a-I), the pitch $\Delta\rho$ gradually increases from the center to the edge, while it can also change in the opposite direction, as shown in Fig. 6(a-II). The variation of the pitch $\Delta\rho$ can also vary in different directions from the center to the edge. Besides the pitch $\Delta\rho$, the angular stepover can also change around the center point, as shown in Fig. 6(a-IV) and 6(a-V). Furthermore, the pitch and angular stepover can change together and the control points in some sections are concentrated, as shown in Fig. 6(a-VI). Similar work can be realized in the mesh method as well. The mesh patterns with different stepovers Δx and Δy along the x- and y-axis based on different surface shape variations are demonstrated in Fig. 6(b). Different from the constant sampling pattern in Fig. 6(b-I), the control points can be concentrated along the x- and y-axis, as shown in Fig. 6(b-II) and 6(b-III). In addition, the patterns can also be modified by changing the Δx and Δy simultaneously to change the density of the control point at different positions, *i.e.,* at the center or corners, as shown in Fig. 6(b-IV) to (b-VI). Therefore, by varying the sampling parameters, the density of the control points at different positions can be precisely adjusted.

[DOI: 10.1299/jamdsm.2023jamdsm0012]

2.4. Experimental setup and conditions

To characterize the ACTS method, two typical kinds of sinusoidal freeform surfaces are utilized for demonstration in both mesh and ring patterns by numerical prediction and fabrication experiments. Since the mesh method is superior in describing the micro-structures in Cartesian coordinates, one sinusoidal freeform surface, employing x and y as function arguments, is adopted, which can be can be expressed as $z(x, y) = A_x\sin(2\pi f_x x) + A_y\sin(2\pi f_y y)$. The amplitude and the spatial frequency are set as $A_x = A_y = 0.5$ μm and $f_x = f_y = 10$ mm^{-1}. While for the ring pattern, the other kind of sinusoidal freeform surface in cylindrical coordinate is employed, which can be mathematically described as $z(\rho, \theta) = A_\rho\sin(2\pi f_\rho \rho) + A_\theta\sin(2\pi f_\theta \theta)$. The amplitude and the spatial frequency are set as $A_\rho = A_\theta = 0.5$ μm, $f_\rho = 100$ mm^{-1} and $f_\theta = 0.05$ °$^{-1}$.

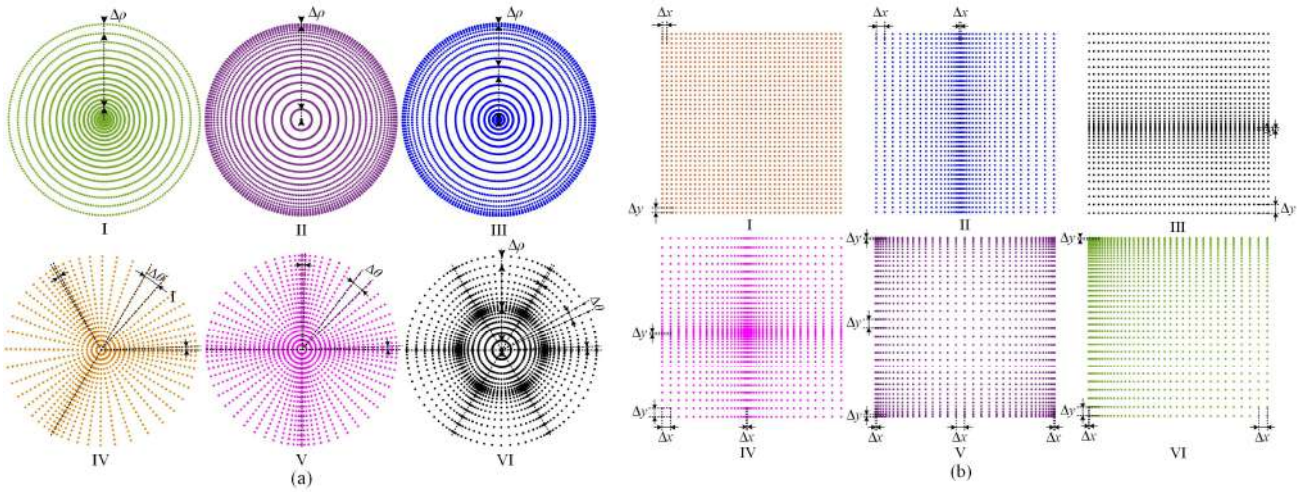

Fig. 6 Schematic diagrams of non-uniform control point sampling in (a) ring patterns and (b) mesh patterns.

The diamond turning cutting tests are performed on a CNC ultra-precision lathe (Nanoform X, AMETEK Precitech Inc., USA) with a commercial FTS unit (FTS-5000, AMETEK Precitech Inc., US). The hardware configuration of the experimental setup is shown in Fig. 7(a). The lathe is equipped with an air-bearing spindle and hydrostatic rotary/linear tables with a nanometric step resolution. The workpiece is installed on the spindle by a vacuum chuck, and the diamond tool is clamped on the FTS turret, which follows the translational motion of the w-axis. The tool used in the experiment is a commercial natural single-crystalline diamond tool (K&Y Diamond Ltd, Canada) with a nose radius of $R_t = 0.083$ mm, a rake angle of 0° and a clearance angle of 14°. The side-feeding rate is set as $f = 5$ μm/rev and 1 μm/rev for the rough and finish cutting. After machining, the machined surface is cleaned with acetone and alcohol to remove the attached chips. An optical profilometer (Nexview N2, AMETEK Zygo Corp., USA) and an optical microscope (OLS4100, Olympus Corp., Japan) are employed to capture the micro-morphologies of the machined freeform surfaces, which are further introduced into the mathematical software for further analysis. The micro-optical images of the machined freeform surface are shown in Fig. 7(b) and 7(c). To observe a large area beyond the measurement range, a set of images are stitched together using the post-processing software. The detailed diamond turning parameters and tool geometry are summarized in Table 1.

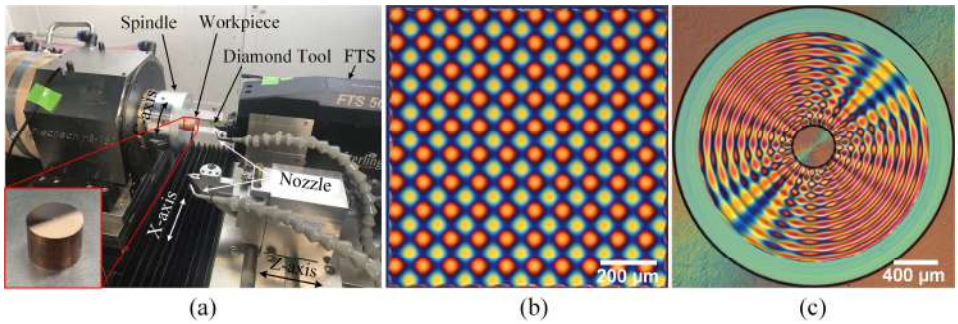

Fig. 7 (a) Hardware configuration of the FTS diamond turning, (b) and (c) the optical images of the machined freeform surfaces in both the mesh and ring patterns.

[DOI: 10.1299/jamdsm.2023jamdsm0012]

Table 1 Diamond turning parameters and tool geometry

Workpiece material	Oxygen-free copper
Workpiece dimension	Φ20 ×15 mm^3
Depth of cut d /μm	5 (Rough cutting) 1 (Finish cutting)
Feed rate f μm/rev	5 (Rough cutting) 1 (Finish cutting)
Spindle rotation N /rpm	50
Cutting tool	Diamond tool
Tool radius R_t /mm	0.083
Rake angle γ_0 /degree	0
Clearance angle α_0 /degree	14
Coolant	Oil mist

3. Result and discussion

3.1. Theoretical prediction of machined surface

In the ACPS optimization, the desired tolerances of the linear interpolation error and initial minimum stepovers are set as $\varepsilon_x = \varepsilon_y = 10$ nm and $\Delta x_{min} = \Delta y_{min} = 50$ nm, which can fulfill the requirements for most optical surfaces. The ACPS method in the mesh pattern and the corresponding freeform surface is shown in Fig. 8(a). In order to have an intuitive comparison, the constant sampling method in the mesh pattern, with the same number of control points, is illustrated in Fig. 7(b). To get a better description of the features of the control point cloud, the projected control point clouds of the ACPS method and the constant sampling method are illustrated in Fig. 8(c) and 8(d). Different from the features of the control point cloud with a constant stepover in Fig. 8(c), the control point cloud of the ACPS method, in Fig. 8(d), possesses variable sampling stepovers, which are closely related to the variation of local surface shape variation. It is noted that more control points are concentrated at the convexity and concavity with drastic curvature variation. Furthermore, the other demonstration sinusoidal freeform surface utilizing a control point cloud in the ring pattern is shown in Fig. 9(a), which belongs to centrosymmetric micro-structures. The corresponding control point cloud optimized by the ACPS method is shown in Fig. 9(b). From the projected control point clouds, the enlarged view indicates that the radial pitch and angular stepover between the adjacent control points are variable with the ACPS method (Fig. 9(c) and 9(d)), while its counterpart holds a constant stepover on the whole machining surface (Fig. 9(e) and 9(f)). By comparing the control point clouds with the ACPS method and the constant sampling method, the ACPS method demonstrates its capabilities and superiorities in adaptation and flexibility for the intricated freeform surface.

3.2. Theoretical investigation of surface generation

For further investigation of the feasibility of the proposed ACPS method, numerical simulation of the freeform surface generation is conducted with both the ACPS method and the constant sampling method in both the mesh and ring patterns to investigate the resulting form error. The diamond tool and desired freeform surface are the same as those in the fabrication experiment stated above.

[DOI: 10.1299/jamdsm.2023jamdsm0012]

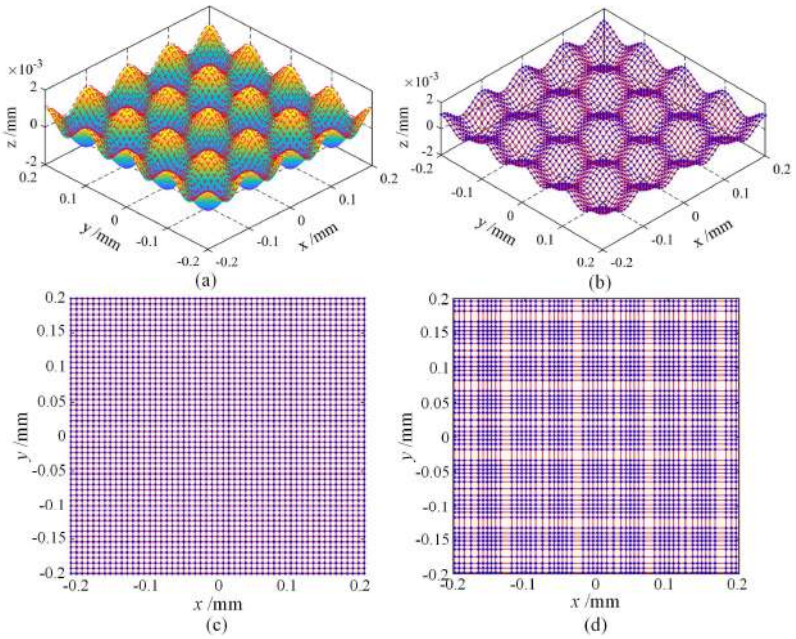

Fig. 8 Schematic diagrams of (a) the sinusoidal freeform surface, (b) the corresponding control point cloud with constant stepover, (c) and (d) the projected control point clouds in the constant sampling method and the ACPS method in the mesh pattern for the freeform surface.

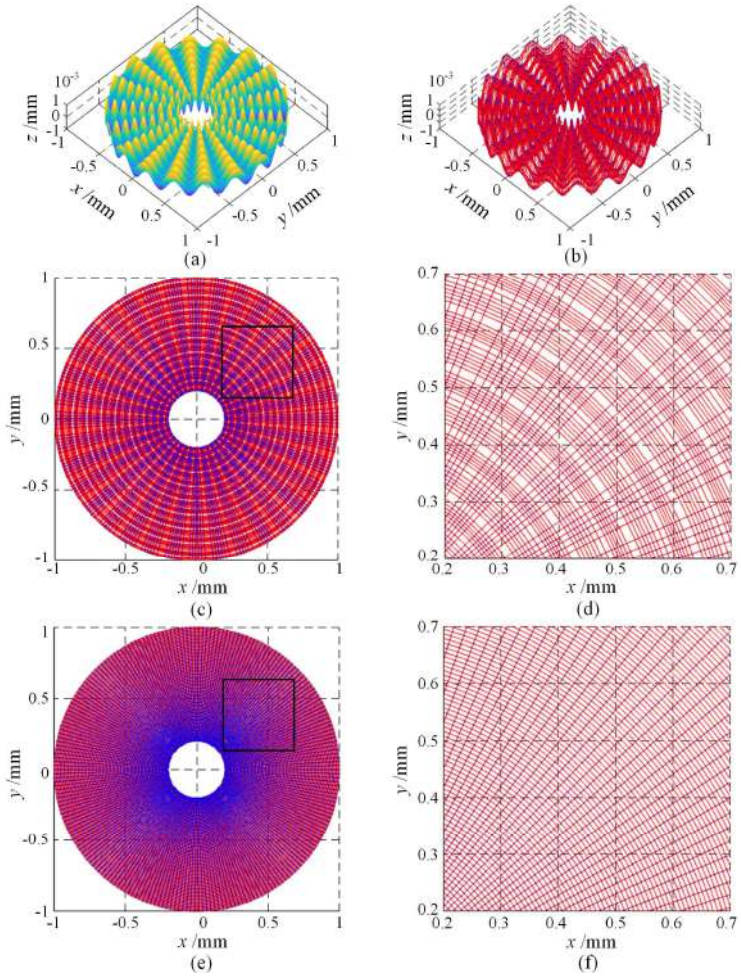

Fig. 9 Schematic diagrams of (a) the sinusoidal freeform surface and (b) the corresponding control point cloud in ring pattern, (c) and (d) the projected and enlarged view of the control point cloud of the ACPS method, (e) and (f) the projected and enlarged view of the control point cloud in the constant sampling method in ring pattern for the freeform surface.

[DOI: 10.1299/jamdsm.2023jamdsm0012]

In the mesh pattern, after removing the desired surface profile, the form error maps by numerical prediction in the ACPS method and the constant sampling method are shown in Fig. 10(a) and 10(b). From the results, the distribution of form error is highly dependent on the surface shape variation. The maximum deviation is concentrated near the concavity or convexity with the maximum curvature in heterogeneous distribution, which agrees well with the theoretical analysis shown in Fig. 3(b) and 3(c). In order to have a clear view of the form error, the obtained error maps are observed from the *x*-*z* plane, as illustrated in Fig. 10(c) and 10(d). By comparison, the form error on the ACPS method surface is restricted to a narrow range within ±19.6 nm. In contrast, from the projected form error map displayed in Fig. 10(d), the form error by the conventional constant sampling method approximately follows harmonic curves, covering a range within ±30.1 nm, which is about 1.5 times larger than that with the ACPS method. This suggested that the ACPS method has primarily improved the surface accuracy by reducing the stepovers near the concavity and convexity, which is only about 65.3 % of the form error induced by the constant sampling method.

A similar measurement is done to investigate the effectiveness of the ACPS method in the ring pattern. Fig. 11(a) and 11(b) show the numerical simulation of the form error maps on the machined surface after subtracting the desired surface. With the ACPS method, not only the form error is constrained within a narrow band between ± 20.1 nm, but the variation of form error is more stable over the machining surface as well. Both the distribution feature and the amplitude range are within the expectation. According to the form error maps in Fig. 11(c) and 11(d), the form error with the constant sampling method is between ± 34.8 nm, much larger than that with the ACPS method, which further confirms the feasibility of the proposed sampling method with the ring pattern on freeform surfaces.

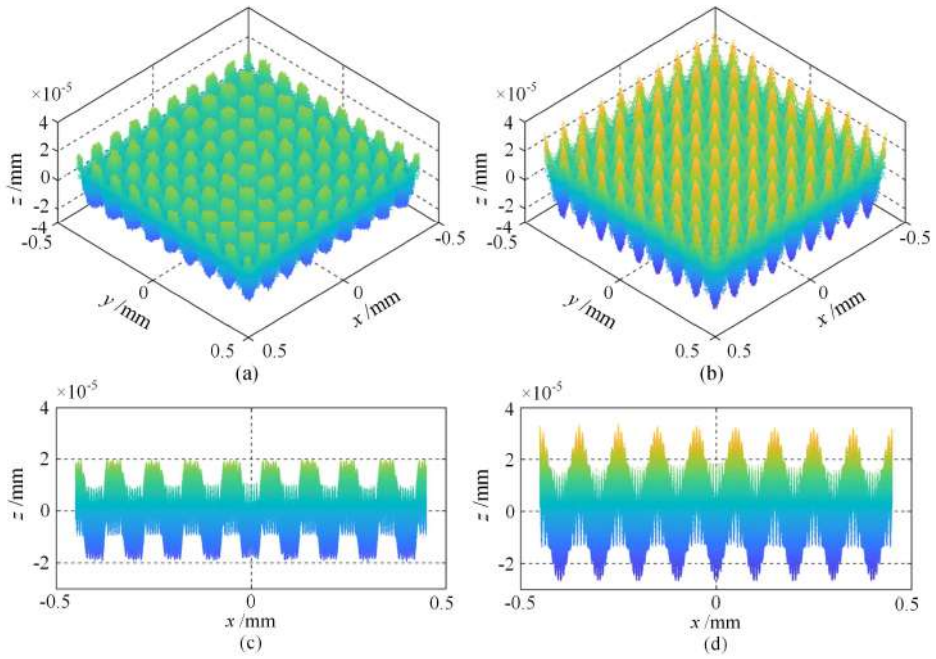

Fig. 10 The 3D morphologies of the form error map in mesh pattern in (a) the ACPS method and (b) the constant sampling method, and the projected error maps in *x*-*z* plane in (c) the ACPS method and (d) the constant sampling method.

3.3. Surface characterization and discussion

To demonstrate the capacity of the sampling method, the machined freeform surfaces in both the mesh and ring patterns using the ACPS method and the constant sampling method are fabricated. The machined freeform surfaces of the ACPS method are captured and stitched together by the optical profilometer, as shown in Fig. 12(a) and 12(b), respectively. From the 3D morphologies shown in Fig. 12, the microstructures over large areas share homogenous features without structure and position distortions. It indicates that homogeneous freeform surfaces are well achieved over the whole machining area in both the mesh and ring patterns.

For further evaluating the form accuracy of the machined surface, an arbitrary region of a single measurement range is further captured with an amplification of 50 ×. The obtained micro-morphologies of the machined surfaces by using the ACPS method and the constant sampling method in the mesh pattern are captured and shown in Fig. 13(a) and 13(b). After removing the desired surface, the corresponding error maps are illustrated in Fig. 13(c) and 13(d). From the obtained

[DOI: 10.1299/jamdsm.2023jamdsm0012]

result, it is clear that a significant reduction of form error is achieved on the machined surface with the ACPS method, which agrees well with the numerical prediction in Fig. 10(a) and 10(c). Furthermore, the comparison also demonstrates the feasibility of the proposed ACPS method for the generation of homogeneous surface quality on intricated freeform surfaces. The positive and negative form errors obtained from the machined surface by the constant sampling method display a high dependence on the concavity and convexity of the freeform surface shown in Fig. 13(d), which is similar to the theoretical prediction result shown in Fig. 10(d). However, the measured PV values results are more significant than the numerical predictions. This is because the numerical predictions are under ideal conditions of diamond turning, without consideration of practical factors that might induce error in the machined surfaces, such as motions of the hardware system and tool shape error (Nagayama and Yan, 2021). In addition, besides the features of the form error stated above, it is noted that the form error is also concentrated inside the gridding pattern, which should be attributed to the control point sampling pattern. Furthermore, in the other case, the micro-morphologies of the machined surfaces using the ACPS method and the constant sampling method in the ring pattern are illustrated in Fig. 14(a) and 14(b), and the corresponding form error maps are presented in Fig. 14(c) and 14(d). From the form error maps, it turns out that many features of form errors between these two cases are identical. Different from the form errors inside the gridding pattern in the mesh pattern, the form error is distributed along the radius in the ring pattern over the whole measured surface.

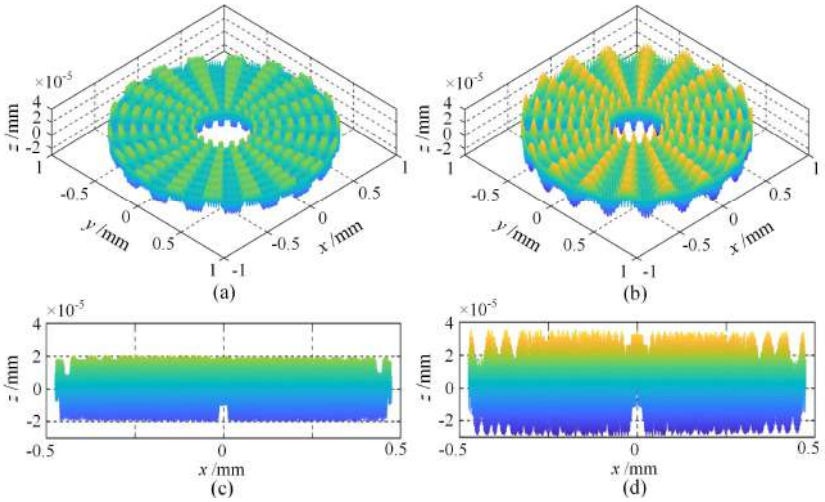

Fig. 11 The 3D morphologies of the form error map in the ring pattern in (a) the ACPS method and (b) the constant sampling method, and the projected error maps in *x*-*z* plane in (c) the ACPS method and (d) the constant sampling method.

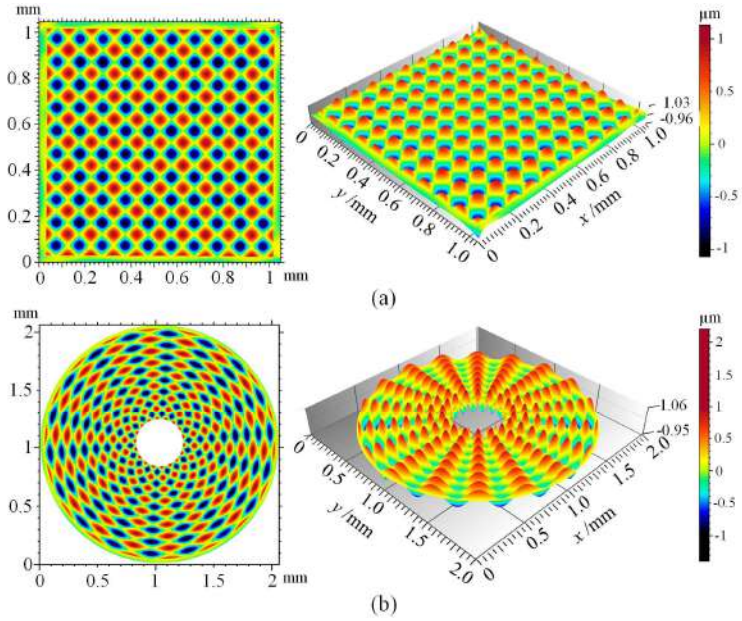

Fig. 12 3D micro-structures of the machined surfaces in the ACPS method in the (a) mesh pattern and (b) ring pattern.

[DOI: 10.1299/jamdsm.2023jamdsm0012]

Some more detailed experimental results on the form error and surface roughness are summarized in Table 2. In the comparison, the number of control points in the ring pattern is 17,161, while that in the ring pattern is 141,512. The PV and RMS values of the form error obtained with the ACPS method are about 35 % smaller than that obtained with the constant sampling method. It indicates that the ACPS method is an efficient method to reduce the volume of the control point cloud in FTS diamond turning without sacrificing form accuracy. In addition, the surface roughness obtained with the ACPS method is slightly smaller than that obtained with the conventional constant sampling method. Based on the above result, it is suggested that the ACPS method is a novel advanced sampling method, which could suppress interpolation error, improve surface quality, and enhance machining efficiency.

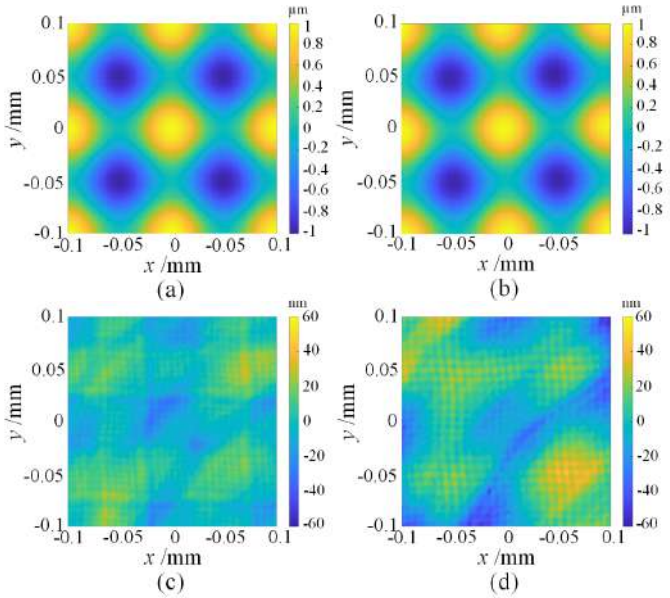

Fig. 13 Measured 3D micro-structure of the machined surfaces in mesh pattern in (a) the ACPS method and (b) the constant sampling method, and the corresponding micro-morphologies after subtracting the desired surface in (c) the ACPS method and (d) the constant sampling method.

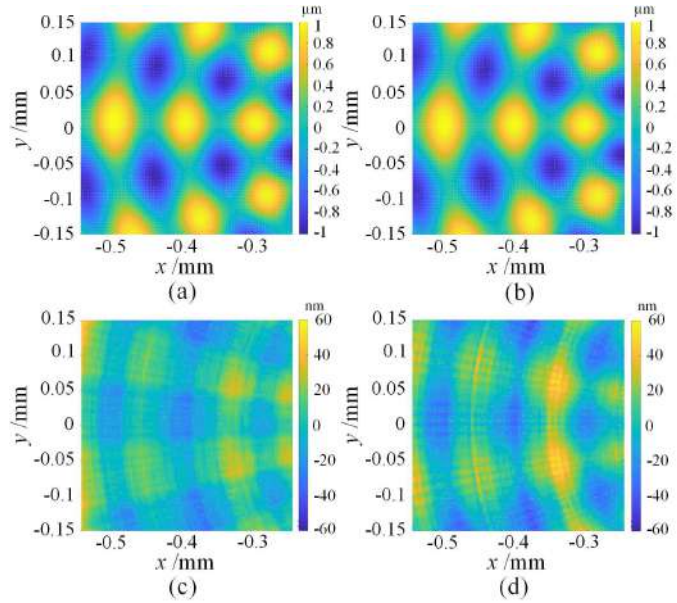

Fig. 14 Measured 3D micro-structure of the machined surfaces in ring pattern in (a) the ACPS method and (b) the constant sampling method, and the corresponding micro-morphologies after subtracting the desired surface by (c) the ACPS method and (d) the constant sampling method.

[DOI: 10.1299/jamdsm.2023jamdsm0012]

Table 2 Surface characteristics of the machined surfaces

Control point pattern	Mesh pattern		Ring pattern	
Sampling method	ACPS	Constant	ACPS	Constant
Number of control point	17,161		141,512	
PV-value /nm	66.5	106.6	84.8	103.2
RMS /nm	11.0	16.9	13.5	17.7
Surface roughness S_a /nm	4.5	5.2	4.8	5.4

4. Conclusions

A novel ACPS method for FTS diamond turning is proposed for the fabrication of intricated freeform surfaces to improve the form accuracy and enhance the machining efficiency simultaneously. Different from the spiral pattern in STS diamond turning, the independent FTS unit utilizes different sampling patterns, including the ring and mesh patterns, for fast search and easy processing. To suppress the interpolation error in two directions, the variable sampling stepovers, adaptive to the surface shape variation, could be precisely achieved. In addition, numerical simulations of the machined sinusoidal freeform surfaces with both the ACPS method and the constant sampling method in the mesh and ring patterns are conducted. The numerical results indicated that the ACPS method could significantly improve surface form accuracy. Finally, by employing a commercial FTS unit, a comparison investigation on surface generation with the ACPS method and the constant sampling method is experimentally conducted on typical sinusoidal freeform surfaces, which presents well agreement with the predicted form error results. Simultaneously, the surface roughness is slightly improved with the ACPS method.

Acknowledgments

Lin Zhang is an International Research Fellow of the Japan Society for the Promotion of Science (JSPS) (ID No. P 20368), and this study has been financially supported by Grant-in-Aid for JSPS Fellows. Jiwang Yan would like to acknowledge the financial support from JSPS Grant-in-Aid for Scientific Research (B), project number 21H01230, and the equipment support from AMETEK Precitech Inc., USA.

References

Bauer, A., and Rolland, J. P., Visual space assessment of two all-reflective, freeform, optical see-through head-worn displays, Optics Express, Vol. 22, No. 11 (2014), pp. 13155-13163.

Dick, L., Risse, S., and Tünnermann, A., Injection molded high precision freeform optics for high volume applications, Advanced Optical Technologies, Vol. 1, No. 1-2 (2012), pp. 39-50.

Fang, F. Z., Zhang, X. D., Weckenmann, A., Zhang, G. X., and Evans, C., Manufacturing and measurement of freeform optics, CIRP Annals, Vol. 62, No. 2 (2013), pp. 823-846.

Gao, W., Araki, T., Kiyono, S., Okazaki, Y., and Yamanaka, M., Precision nano-fabrication and evaluation of a large area sinusoidal grid surface for a surface encoder, Precision Engineering, Vol. 27, No. 3 (2003), pp. 289-298.

Jiang, X., Scott, P., and Whitehouse, D., Freeform Surface Characterisation - A Fresh Strategy, CIRP Annals, Vol. 56, No. 1 (2007), pp. 553-556.

Kim, D. W., Smith, G. A., Dubin, M., Lowman, A., Oh, C.-j., Quach, H., Kang, H., Yoo, H., Trumper, I., Graves, L., Aftab, M., Davila-Peralta, C., Hyatt, J., and Choi, H., Advances in reconfigurable optical design, metrology, characterization, and data analysis, Journal of Physics: Photonics, Vol. 3, No. 2 (2021), pp. 022003.

Kim, H.-S., Lee, K.-I., Lee, K.-M., and Bang, Y.-B., Fabrication of free-form surfaces using a long-stroke fast tool servo and corrective figuring with on-machine measurement, International Journal of Machine Tools and Manufacture, Vol. 49, No. 12 (2009), pp. 991-997.

Lu, X., and Trumper, D. L., Spindle rotary position estimation for fast tool servo trajectory generation, International Journal of Machine Tools and Manufacture, Vol. 47, No. 9 (2007), pp. 1362-1367.

[DOI: 10.1299/jamdsm.2023jamdsm0012]

Nagayama, K., and Yan, J., Deterministic error compensation for slow tool servo-driven diamond turning of freeform surface with nanometric form accuracy, Journal of Manufacturing Processes, Vol. 64, No. (2021), pp. 45-57.

Neo, D. W. K., Kumar, A. S., and Rahman, M., A novel surface analytical model for cutting linearization error in fast tool/slow slide servo diamond turning, Precision Engineering, Vol. 38, No. 4 (2014), pp. 849-860.

Roland, G., Eric, R., Remi, B., Renaud, M.-Y., Hervé, L., and Francois, R., Freeform optics design, fabrication and testing technologies for Space applications, International Conference on Space Optics (ICSO 2018) (2019), Paper No. 11180.

Sato, Y., and Yan, J., Tool path generation and optimization for freeform surface diamond turning based on an independently controlled fast tool servo, International Journal of Extreme Manufacturing, Vol. 4, No. 2 (2022), pp. 025102.

Scheiding, S., Yi, A. Y., Gebhardt, A., Li, L., Risse, S., Eberhardt, R., and Tünnermann, A., Freeform manufacturing of a microoptical lens array on a steep curved substrate by use of a voice coil fast tool servo, Optics Express, Vol. 19, No. 24 (2011), pp. 23938-23951.

Tanikawa, S., and Yan, J., Fabrication of micro-structured surface with controllable randomness by using FTS-based diamond turning, Precision Engineering, Vol. 73, No. (2022), pp. 363-376.

Yu, D. P., Gan, S. W., Wong, Y. S., Hong, G. S., Rahman, M., and Yao, J., Optimized tool path generation for fast tool servo diamond turning of micro-structured surfaces, The International Journal of Advanced Manufacturing Technology, Vol. 63, No. 9 (2012), pp. 1137-1152.

Yu, D. P., Wong, Y. S., and Hong, G. S., Optimal selection of machining parameters for fast tool servo diamond turning, The International Journal of Advanced Manufacturing Technology, Vol. 57, No. 1 (2011), pp. 85-99.

Zhang, H., Li, L., McCray, D. L., Scheiding, S., Naples, N. J., Gebhardt, A., Risse, S., Eberhardt, R., Tünnermann, A., and Yi, A. Y., Development of a low cost high precision three-layer 3D artificial compound eye, Optics Express, Vol. 21, No. 19 (2013), pp. 22232-22245.

Zhang, L., Hashimoto, T., and Yan, J., Machinability exploration for high-entropy alloy FeCrCoMnNi by ultrasonic vibration-assisted diamond turning, CIRP Annals, Vol. 70, No. 1 (2021), pp. 37-40.

Zhou, M., Zhang, H. J., and Chen, S. J., Study on Diamond Cutting of Nonrationally Symmetric Microstructured Surfaces with Fast Tool Servo, Materials and Manufacturing Processes, Vol. 25, No. 6 (2010), pp. 488-494.

Zhu, Z., and To, S., Adaptive tool servo diamond turning for enhancing machining efficiency and surface quality of freeform optics, Optics Express, Vol. 23, No. 16 (2015), pp. 20234-20248.

Zhu, Z., To, S., and Zhang, S., Large-scale fabrication of micro-lens array by novel end-fly-cutting-servo diamond machining, Optics Express, Vol. 23, No. 16 (2015), pp. 20593-20604.

[DOI: 10.1299/jamdsm.2023jamdsm0012]